

LASERS

PACS numbers: 42.55.Vc; 42.65.Re; 52.38.Ph
DOI: 10.1070/QE2012v042n12ABEH014935

Subpicosecond 41.8-nm X-ray laser in the plasma produced by femtosecond laser irradiation of a xenon cluster jet

E.P. Ivanova

Abstract. **Model calculations are performed of the radiation gain for the 4d5d ($J = 0$)–4d5p ($J = 1$) transition with a wavelength of 41.8 nm in Pd-like xenon ions in the plasma produced by femtosecond laser irradiation of a xenon cluster jet. Conditions for the excitation of an ultrashort-pulse (~1 ps) X-ray laser are discussed.**

Keywords: *X-ray laser simulations, atomic kinetic calculations, Pd-like xenon ion.*

1. Introduction

At present, the search is on for ways of obtaining holographic diffraction images with a high spatiotemporal resolution for visualising rapidly varying nanoobjects. In particular, modern free-electron X-ray lasers (XRLs) with a radiation wavelength $\lambda = 1-10$ nm and a pulse duration $t_{las} = 15$ fs permit recording the holographic images of intermediate nanoobject states in a time comparable to the time of atomic motion [1, 2]. Recent papers [1, 2] showed the feasibility of observing the dynamics of phase transitions in solids: formation of cracks, nucleation of phases and their separation, fast fluctuations in liquids and biological cells. High-power XRLs with a subpicosecond pulse duration may be validly employed for the diagnostics of rapidly varying laser plasma in the critical density region.

For many applications, use can be made of compact XRLs with sufficiently short output wavelengths and a pulse duration below 1 ps. A basic requirement is that the images of nanoobjects should be obtained in one pulse, which requires that the number of outgoing photons should be no less than 10^{12} per each XRL pulse.

The basic prerequisites to the development of ultrashort-pulse XRLs were developed in Refs [3–8], where the plasma was produced by a laser prepulse, which was followed by an ultrashort pulse producing a large population inversion between the working levels. In this scheme, use can be made of the pulses of two lasers; however, the use of a high-order harmonic (HOH) pulse with a wavelength close to the output XRL wavelength has turned out to be most efficient (the HOH may be produced in the nonlinear conversion of femtosecond laser radiation using the transition of a specially selected atomic gas. The duration of the output XRL radiation pulse is defined by the pump parameters and the plasma density.

With the use of an ultrafast streak camera, in 2002 measurements were made of the time-resolved energy output of $\lambda = 13.9$ nm XRL radiation arising from the 4d ($J = 0$) – 4p ($J = 1$) transitions of Ni-like silver ions (Ag^{19+}) [3]. Under optimal pumping conditions, the temporal half-amplitude width of an XRL pulse was equal to 1.9 ± 0.7 ps and its energy amounted to 2–6 μJ. The delay between the long prepulse (300 ps, $\sim 10^{12}$ W cm^{-2}) and the main pulse (1.3 ps, 1.1×10^{15} W cm^{-2}) was equal to 200 ps. In Ref. [3] it was determined that the highest XRL output (E_{out}) was reached earlier than the highest electron plasma temperature. Proceeding from this fact as well as from the data of time-resolved spectroscopic measurements, a conclusion was drawn that the gain lowered due to ionisation of the working ion Ag^{19+} to higher charge states (Ag^{20+}, Ag^{21+}, etc.).

In 2009, with the use of an ultrafast streak camera the temporal width of an XRL pulse was estimated at 1.13 ± 0.47 ps [9]. The study of Ref. [9] was concerned with the investigation of an XRL ($\lambda = 32.6$ nm) on Ne-like titanium ions, where the working medium was produced by three sequential pump pulses: A 120-ps long prepulse with an energy of 10 mJ, the second prepulse with an energy of ~350 mJ delayed by 5 ns relative the first one (both prepulses were focused nearly along the normal to the titanium target surface), and the third 6.7-ps long heating pulse with an energy of 0.9 J directed at a grazing angle of 23°. As a result, the working plasma with a density of $\sim 10^{20}$ cm^{-3} was produced for the amplification at $\lambda = 32.6$ nm in Ne-like titanium ions. The remaining part of Ti:sapphire laser radiation was employed to generate the 25th harmonic radiation, which was directed to the active medium at an angle of 9°. The wavelength of this harmonic generated in gaseous argon was hardly different from the working wavelength $\lambda = 32.6$ nm. Its interaction with the XRL radiation resulted in a significant improvement in the coherence of XRL radiation [9]. A similar scheme was used in Ref. [6], where it was possible to reach gain saturation at XRL wavelengths in Ni-like ions of molybdenum ($\lambda = 18.9$ nm) and silver ($\lambda = 13.9$ nm). Both XRLs were induced by the HOHs at the corresponding wavelengths. High intensity short XRL radiation pulses were obtained, which exhibited an extremely high spatial coherence and a low divergence. Furthermore, owing to the small spectral width of these pulses the spectrum of HOH pulses became narrower, i.e. their temporal coherence was improved.

The possibility in principle of achieving complete spatial coherence of XRL radiation with the use of a HOH pulse was demonstrated in Ref. [4]. The main problem consisted in producing the HOH beam of high optical quality. An investiga-

E.P. Ivanova Institute for Spectroscopy, Russian Academy of Sciences, ul. Fizicheskaya 5, 142190 Troitsk, Moscow, Russia;
e-mail: eivanova@isan.troitsk.ru

Received 3 July 2012; revision received 4 October 2012
Kvantovaya Elektronika **42** (12) 1100–1105 (2012)
Translated by E.N. Ragozin

tion was made of an XRL on the 4d ($J = 0$)–4p ($J = 1$) transition of Ni-like krypton ions with $\lambda = 32.8$ nm in the plasma produced by optical field ionisation (OFI) of gaseous krypton. The HOH pulse was delayed so that it was focused into the working plasma volume at the moment the gain was at its maximum.

The plasma is produced by OFI under longitudinal target pumping; a strong gradient of the refractive index appears in the working medium because of a lower electron density at the plasma edge. In this connection, different waveguide schemes are developed for the XRL plasma to improve its uniformity and lower the divergence of the output short-wavelength radiation. In particular, a 400-fold increase in the $\lambda = 32.8$ nm radiation energy output of a Kr IX ion XRL was attained by using an axicon to form a waveguide.

Recent years have seen the development of a new line of XRL research, which involves the OFI of krypton (Kr IX, $\lambda = 32.8$ nm [10, 11] and xenon (Xe IX, $\lambda = 41.8$ nm) [12]) cluster jets. Ultrashort-pulse XRLs were not produced in this case, but the resultant data may be employed for their development. In particular, an original experimental scheme was developed [11], whereby the amplified spontaneous $\lambda = 32.8$ nm Kr IX emission interacts during its propagation with the HOH radiation of the same wavelength, which propagates in the same direction. In Ref. [11] the krypton cluster jet was formed by a slit nozzle; the plasma was pumped by irradiating clusters along the slit direction. The plasma parameters were as follows: $L = 8$ mm length, $d = 25$ μm diameter, $n_i = 1.6 \times 10^{19}$ cm^{-3} ion density, $n_e \approx 10^{20}$ cm^{-3} electron density. The plasma was pumped by three sequential Ti : sapphire laser pulses (10 TW, 38 fs, 810 nm, 10 Hz). The first circularly polarised radiation pulse (235 mJ, 38 fs) was employed to prepare by OFI technique the plasma dominated by the Kr IX working ions. In 2.5 ns this pulse was followed by two other pulses – an 'igniter' (45 mJ, 38 fs, linear vertical polarisation) and a 'heater' (270 mJ, 160 ps, linear horizontal polarisation), which were used for plasma waveguide formation. The time interval between them was equal to 200 ps. An optical scheme was developed for radiation focusing, which comprised an axicon for plasma waveguide formation [10]. In the thus produced XRL, a spatially uniform plasma density distribution was prepared. In this case, the wavelength of the 25th Ti : sapphire laser radiation harmonic generated in a neutral argon jet coincides closely with the wavelength of XRL radiation. The optimal time delay of the HOH pulse relative to the onset of X-ray lasing was equal to 2 ps. These parameters of the pulses provided a maximum photon output of 10^{11} photons pulse^{-1}. Using the 25th harmonic resulted in a 4.5-fold decrease in XRL radiation divergence. In this case, measurements of the spatial coherence performed using a two-slit Young interferometer showed that it became ~4 times higher. The use of the HOH raised the photon output by 10%.

The stimulation of XRL emission under resonance interaction of the HOH of femtosecond laser radiation with an inverted working transition is a unique instrument for measuring the time of gain existence in the XRL. This method was demonstrated in Ref. [13], where a procedure was developed for measuring the XRL gain as a function of time. By varying the time delay between the instant of XRL medium formation and the arrival of the HOH pulse it is possible to trace the time evolution of the XRL gain with a time resolution of several femtoseconds. In Ref. [13], measurements were made of the time-dependent gain factors in Xe^{8+} (Pd-like xenon ion, $\lambda = 41.8$ nm). The plasma was produced by OFI of gaseous xenon. The time dependences of the gain were given for gaseous xenon pressures of 5–25 Torr (Figs 2–4 in Ref. [13]); in this case, the time of XRL gain existence shortened from 34.1 to 5.5 ps.

The technique developed in Ref. [13] is efficient for verifying theoretical models and the atomic data values employed. The results of this work are in good agreement with our simulations of the time evolution of the gain in Xe^{8+}, which were performed in Refs [14, 15] prior to the execution of the experiment of Ref. [13]. Our simulations [14–17] suggest that the lowering of XRL gain is due to the ionisation of Xe^{8+} to higher charge states (Xe^{9+}, Xe^{10+}). The duration of the output XRL radiation pulse shortens with increasing electron density as $\sim 1/n_e$, which is also confirmed by the experiment of Ref. [13].

We note that the resonance interaction of the HOH with the XRL working transition radiation may lead to an increase in HOH intensity. In particular, in the experiment of Ref. [6] measurements were made of the radiation parameters for an XRL on Ni-like silver ions ($\lambda = 13.9$ nm). Improvement of the $\lambda = 13.9$ nm XRL radiation coherence was induced by the 59th harmonic of Ti:sapphire laser radiation produced in neon, whose energy output was also measured. Upon the interaction, a 400-fold increase in HOH-pulse energy (up to 75 nJ) was recorded in Ref. [6].

The idea of making an XRL with an ultrashort pulse duration relies on the fact that the pulse duration becomes shorter than 1 ps with increasing electron density. In this case, the average value of the gain may range up to several hundred inverse centimetres, so that the gL product (g is the time-averaged gain and L is the length of the plasma filament) will be sufficient for providing a high XRL photon output even for $L \approx 300$ μm. Increasing the electron density increases the upper level excitation rate, the population inversion, and the gain, and the ionisation rate of the working ion also rises. On the other hand, as the plasma density becomes higher, the reabsorption of photons lowers the depopulation rate of the lower working level, with the consequential lowering (quenching) of the population inversion.

In the present work, we calculate the energy output for a Xe^{8+} XRL for different plasma parameters for the purpose of determining optimal XRL schemes with subpicosecond pulse duration. The proposed scheme involves the use of one pump pulse, an axicon, and a HOH. It is noteworthy that the XRL experiment schemes of Refs [3–8] described above are quite low in efficiency, because they make use, as a rule, of several pump prepulses with a high energy.

2. Prerequisites to the development of an ultrashort-pulse XRL in the plasma produced in the interaction of a laser pump with a xenon cluster jet

The prospect of making an XRL with a subpicosecond pulse duration relies primarily on the anomalously large cross section for the excitation of the upper working level 4d5d ($J = 0$) in Xe^{8+}. The electron impact excitation rate coefficient for this level as a function of temperature was given in our earlier paper [16]. This rate coefficient is approximately three orders of magnitude higher than that for the upper working level $2p^5 3p$ ($J = 0$) of Ne-like argon ions (Ar^{8+}).

In the first Xe^{8+} XRL experiment, large values were obtained for the gL product ($\sim$10) and the pulse duration $t_{las} \geqslant 20$ ps [18]. The plasma was pumped by the OFI of gaseous xenon in a cell. Even higher gL values were achieved in similar experiments that followed [19].

In the experiment of Ref. [12], a high-intensity emission at $\lambda = 41.8$ nm was observed under pumping by a single pulse (without a prepulse) with the use of a slit nozzle, which served to produce a cluster jet. A Ti : sapphire laser system (10 TW, 55 fs, 810 nm) was employed for OFI plasma pumping. The half-height width of the focal spot was equal to 25 μm, which contained 85 % of the pump energy. The peak intensity $I_{pump}^{max} = 7 \times 10^{17}$ W cm^{-2} for a pump energy of 350 mJ. The plasma length – the diameter of the cluster jet – was fixed: $L = 1.7$ mm. The highest output (95×10^{-9} J) was observed for $n_i = 7.5 \times 10^{17}$ cm^{-3} and $n_e \approx 6 \times 10^{18}$ cm^{-3} (see Fig. 3 in Ref. [12]).

XRL radiation pulses were recorded for an atomic density varied by a factor of 300: $1.1 \times 10^{17} \leqslant n_i \leqslant 3.3 \times 10^{19}$ cm^{-3}. The xenon pressure in the stagnation chamber was varied in the 0.013 – 4 MPa (0.13 – 40 atm) range; in this case, and the average cluster size increased from 50 to 500 Å.

We give the main merits of an XRL involving cluster jets:

(1) The capability of absorbing more than 90% of the pump energy; this was demonstrated, for instance, in the experiment of Ref. [20] for rare-gas cluster jets for a peak pump intensity below 10^{17} W cm^{-2}.

(2) Weak reflection of the pump beam from a cluster jet and the absence of debris from the plasma.

(3) The possibility of attaining electron energies as high as several kiloelectronvolts [21]. In other early experiments [22] it was determined that a high electron temperature T_e is achieved in the irradiation of sufficiently large clusters: $T_e > 1$ keV for a cluster diameter of 150 Å and an intensity of $\sim 10^{16}$ W cm^{-2}, and $T_e \sim 10$ keV on increasing the intensity to 5×10^{16} W cm^{-2} (see Fig. 9 in Ref. [22]).

(4) The possibility of controlling the plasma density and temperature as well as the charge-state distribution of the plasma.

(5) For a high velocity of the cluster jet, the XRL pulse repetition rate may range up to ~125 kHz [23].

A large number of parameters that characterise (i) the plasma and its geometry, (ii) the nozzle, the gas pressure in the stagnation chamber, and the cluster size, (iii) and the laser pump pulse should be matched using a theoretical model. Then it will be possible to produce the active medium by a single principal pump pulse. This is possible when the model adequately reproduces experimental data.

The experimental data of Ref. [12] were interpreted in Ref. [16] for the purpose of determining the electron temperature for each experimental atomic density; the value of T_e was selected in such a way as to reproduce the experimental curve in Fig. 3 of Ref. [12]. The density dependence of T_e determined in this way was plotted in Fig. 4 of Ref. [16]. One can see from this Figure that the temperature T_e rose from 300 to 1000 eV with increasing atomic density from 10^{17} to 8×10^{18} cm^{-3}. At higher densities, the XRL output was too low [12].

The cluster size is critically important for producing the high-temperature plasma in the interaction of an ultrashort pump pulse with a cluster jet. The pulse pedestal duration is usually equal to several nanoseconds; in the course of pulse pedestal–cluster interaction the clusters are heated, electrons are ejected from their surface, and the clusters expand. The highest T_e value in the cluster nanoplasma is achieved when $n_e = 3n_{cr}$ [$n_{cr} = \pi c^2 m_e/(e^2\lambda^2)$]; in this case there occurs a resonance energy input into the plasma [20–22]. To maximise the energy input, the pedestal duration and intensity should correspond to the cluster size: when the cluster is too small (rapidly expands to $n_e \sim 3n_{cr}$), its disintegration takes place too early (prior to the arrival of the main high-intensity pulse) and the temperature T_e is not high. When the cluster is too large (expands for too long a time), its disintegration takes place after the passage of the high-intensity pulse, and its temperature T_e is also not high. For the cluster of requisite size, n_e lowers to $3n_{cr}$ at the instant of arrival of the main femtosecond pulse, and T_e is highest in this case.

The dependences of cluster size on the pressure and temperature of gas in the stagnation chamber as well as on the nozzle geometry have been much studied for conic nozzles of circular section, for which the number atoms in rare-gas clusters is usually determined by Rayleigh scattering technique with the use of an empirical formula [24]. Recently a start has been made on the investigation of how the cluster size depends on the stagnation gas pressure for a slit nozzle. In particular, in Ref. [25] it was shown that a supersonic slit nozzle provides a substantially higher number of atoms in a cluster in comparison with a conic nozzle. This circumstance explains the high intensity of the XRL pulse obtained using a single pump pulse and a slit nozzle in Ref. [12].

The plasma electron and ion energies as functions of cluster size were investigated in many experimental works, for instance in Refs [21, 26]. In Ref. [21], a xenon cluster jet was irradiated by laser radiation with a peak intensity of 10^{16} W cm^{-2}. In this work it was shown that the clustering of xenon atoms sets in with increasing stagnation pressure for a pressure of ~1 bar. With increasing pressure the cluster size becomes larger, which results in a rapid growth of the electron plasma temperature (see Fig. 2 in Ref. [21]). The density dependence of T_e is in qualitative agreement with that obtained in Ref. [16]. To extrapolate this dependence to the domain of higher plasma ion densities ($n_i \geqslant 10^{18}$ cm^{-3}, which corresponds to a cluster size of no less than 10^3 atoms cluster^{-1}), we take advantage of Fig. 4 from Ref. [26]. The dependence of T_e on n_i resulting in this case is plotted in Fig. 1. The inset in Fig. 1 shows the

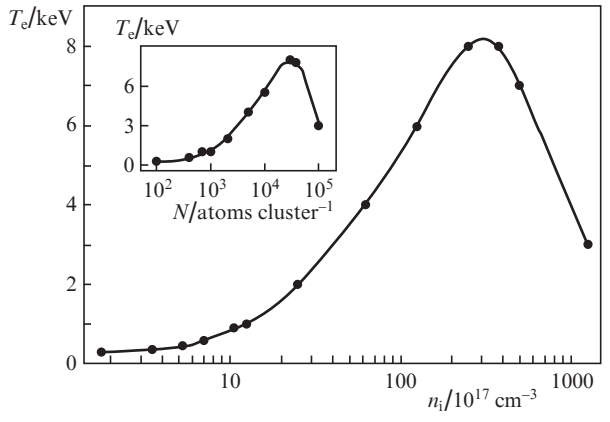

Figure 1. Plasma electron temperature T_e as a function of Xe^{8+} density (n_i). The initial portion of the curve, up to $n_i \sim 6 \times 10^{18}$ cm^{-3}, was calculated in Ref. [16]; the remaining portion was determined with the use of experimental and theoretical data of Ref. [26]. The inset shows the dependence of the plasma electron temperature on the number N of atoms in a cluster (on the cluster size).

corresponding dependence of T_e on the cluster size. We shall use this dependence in the calculation of the gain $g(t)$.

3. Subpicosecond Xe^{8+} ion laser with $\lambda = 41.8$ nm

The model for calculating the XRL operation was employed in our previous works [14–17], which give references to the detailed description of our theoretical approach. In our calculations the plasma was assumed to be a uniform cylinder of diameter $d = 25$ μm, and T_e, T_i were assumed to be constant during amplification (T_i is the ion temperature). The density of Pd-like Xe^{8+} ions immediately after OFI amounts to 0.9 of the total ion density n_i for a laser pump intensity of $10^{16}-10^{17}$ W cm^{-2} [18]. As a result of the tunnel ionisation of xenon atoms, as determined in Ref. [18], the outer 5l electrons are detached and almost 100% of the ions find themselves in the state with a closed $4d^{10}$ shell. In our work [16] the initial Xe^{8+} ion density was determined from the experimental dependences of the photon yields on the plasma filament length [18, 19]. Furthermore, also determined in Ref. [16] was the effective plasma diameter. The calculations of Ref. [16] showed that the initial Xe^{8+} density in the experiments of Refs [18, 19] was equal to ~0.9 and 0.85, respectively. The OFI of a gaseous target provides a low ion temperature T_i [13, 18, 19], so that its effect on the laser transition linewidth is negligible; in this case, T_e may be equal to 100–300 eV [13, 18, 19]. When a cluster jet is employed as a target, the plasma heating results from the explosion of ionised clusters; initially, after the explosion, $T_i \gg T_e$, but the electron-ion thermalisation proceeds in a time no longer than 100 fs for the high plasma density involved ($n_i \geqslant 10^{19}$ cm^{-3}). That is why in the present calculation we assume that $T_e = T_i$. This condition has a strong effect on the Doppler contribution to the laser transition linewidth; at high densities ($n_i \geqslant 10^{19}$ cm^{-3}) the line broadening caused by collisions with electrons nevertheless exceeds the Doppler broadening.

To compare the results of our $g(t)$ calculations with the experimental data of Ref. [13], where the plasma was produced by the OFI of atomic xenon in a cell, we give Fig. 2. This Figure shows the time dependences of g for the $\lambda = 41.8$ nm line of Xe^{8+}. Like the experiment of Ref. [13], our calculation was performed for $T_e = 300$ eV and different pressures of atomic gaseous xenon ($T_i \ll T_e$). In our calculation the plasma diameter $d = 25$ μm; in this case, its variation in the range between 20 and 50 μm has no appreciable effect on the result. A comparison of Fig. 2a of the present work with Fig. 4 from Ref. [13] shows a very close agreement concerning pulse durations, the peak values of $g(t)$, as well as the curve shapes. Our preliminary calculations of $g(t)$ were given in Ref. [15]. The data reported in our work confirm our inference about the output XRL pulse duration t_{las} drawn in our earlier papers [14–17]: t_{las} shortens with increasing plasma density as $\sim 1/n_i$.

Figure 2b shows the results of similar calculation of $g(t)$ performed for the same atom number densities as in Fig. 2a, but in this case the plasma is assumed to result from the OFI of a xenon cluster jet. The temperature T_e is determined according to Fig. 1, and $T_i = T_e$. The changes in the form of dependences in Fig. 2b in comparison with those in Fig. 2a are caused by two factors: an increase in the linewidth due to an enhancement of the Doppler effect and due to an increase in population inversion and gain owing to an increase in T_e with increasing n_i. For low plasma densities ($n_i \leqslant 10^{18}$ cm^{-3}, $T_e \leqslant 1000$ eV) the effect of line broadening prevails, and therefore the $g(t)$ dependence lies below the corresponding curves in Fig. 2a. At higher densities ($n_i \geqslant 5 \times 10^{18}$ cm^{-3}, $T_e \geqslant 5000$ eV) there prevails the effect of rapid population of the upper working level, with the result that the peak values of the $g(t)$ coefficient exceed the corresponding values in Fig. 2a.

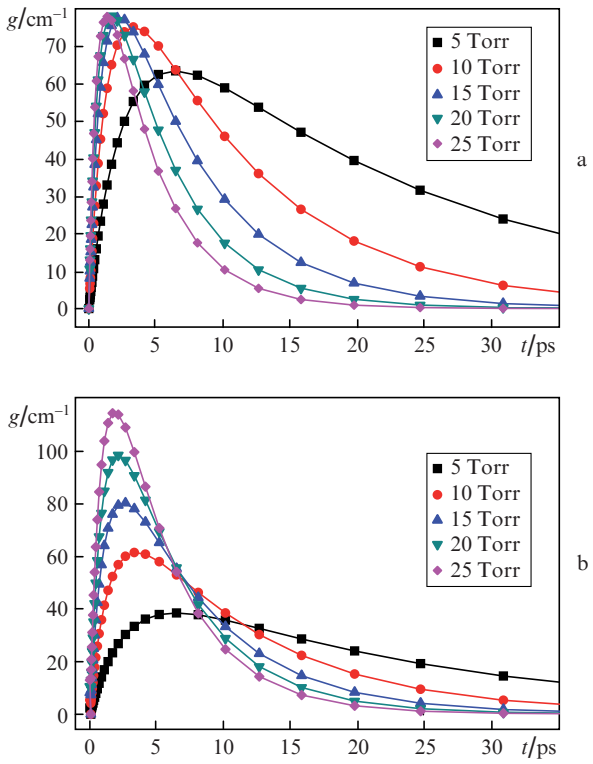

Figure 2. Time dependences of the gain on the Xe^{8+} ion transition with $\lambda = 41.8$ nm in the plasma produced by the OFI of gaseous xenon for $T_e = 300$ eV, gas pressures of 5, 10, 15, and 20 Torr, and ion densities $n_i = 1.75 \times 10^{18}$, 3.5×10^{18}, 5.25×10^{18}, 7.0×10^{18}, and 8.25×10^{18} cm^{-3}, respectively (a), as well as in the plasma produced by the OFI technique in a xenon cluster jet for the same pressures and the electron temperatures $T_e = 300$, 350, 450, 600, and 750 eV, respectively (b).

The dependences plotted in Fig. 3a were calculated for high-density plasmas [$(6.25-43.75) \times 10^{18}$ cm^{-3}, $T_e = 4-8$ keV] assuming an ultrashort pump pulse ($t_{pump} < 100$ fs). One can see that for $n_i \geqslant 3 \times 10^{19}$ cm^{-3} the decay time is equal to ~1 ps and the target length L may be equal to only ~300 μm; this is due to the energy and conditions of the pumping as well as to the desired t_{las}. The quantum $\lambda = 41.8$ nm photon outputs (N_{out}^{ph}) as functions of the target length are shown in Fig. 3b. We note that all the curves approach constant asymptotes, because the radiation loss is neglected for so short a time. The plasma parameters that correspond to the highest output $N_{out}^{ph} \approx 1.7 \times 10^{13}$ photons pulse^{-1} for $t_{las} \approx 1$ ps are as follows: $L \approx 300$ μm, $n_i = 2.5 \times 10^{19}$ cm^{-3}, $T_e = 8$ keV. Figure 4 shows how the photon output N_{out}^{ph} from the plasma volume $V = \pi(d/2)^2 L \approx 1.5 \times 10^{-8}$ cm^3 in a time of 1 ps depends on n_i. One can see that the optimal conditions for the subpicosecond laser utilising the technique of OFI of xenon clusters correspond to a rather narrow atomic density range: $(2.25-2.75) \times 10^{19}$ cm^{-3}.

Evidently, to cut off the afterglow 1 ps after the onset of lasing at $\lambda = 41.8$ nm requires developing a shutter at the plasma output.

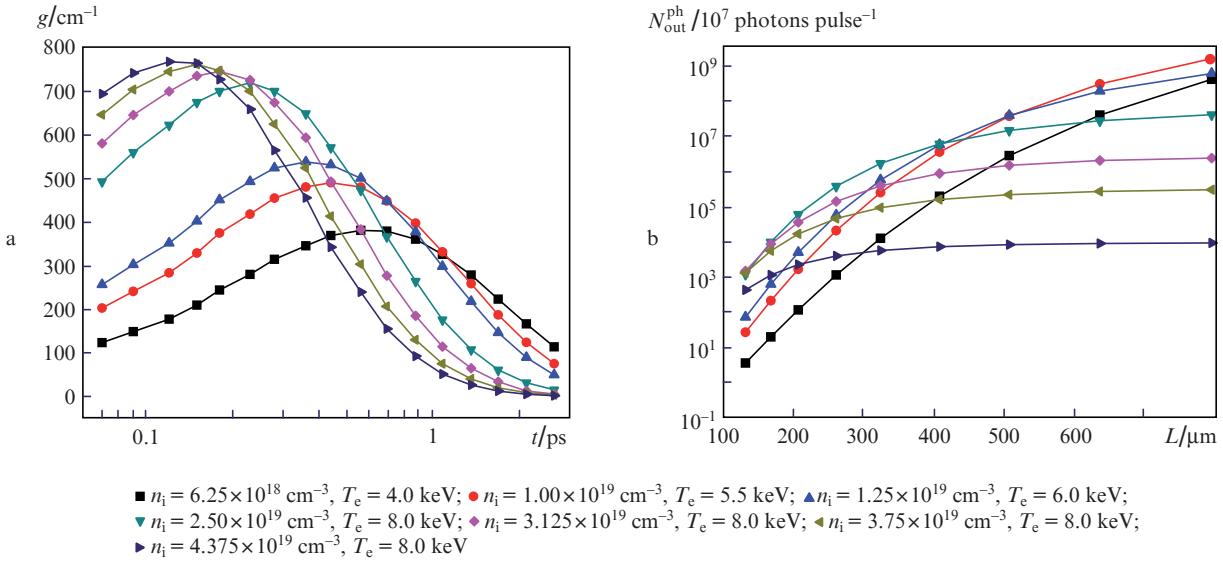

Figure 3. Time dependences of the gain (a) and dependences of the photon output on the plasma length (b) for an XRL with $\lambda = 41.8$ nm and an ultrashort pulse duration for different densities n_i and temperatures T_e.

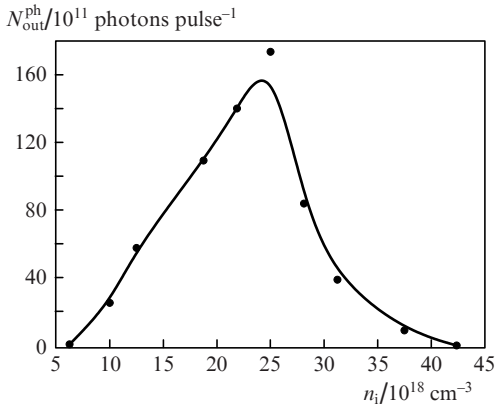

Figure 4. Photon output for an XRL with a pulse duration of ~1 ps as a function of ion density.

4. Conclusions

Three fundamental conditions underlie ultrashort-pulse Xe^{8+} XRL scheme with the $\lambda = 41.8$ nm: a rapid excitation of the $4d^95d$ ($J = 0$) upper laser level from the $4d^{10}$ ground state; a fast ionisation of Xe^{8+} to higher charge states (Xe^{9+}, Xe^{10+}); a high gain g averaged over the 1-ps time interval.

The charge state distribution is determined by the intensity of pump laser radiation; in particular, an intensity of 10^{16}–10^{17} W cm^{-2} would be sufficient to produce plasmas dominated by Xe^{8+} ions. Ordinary femtosecond lasers generate a prepulse of duration several nanoseconds, which should be matched to the cluster size for maximising the energy input from the main femtosecond pulse. To obtain a high-temperature plasma, the average cluster size should be equal to ~500 Å; such a cluster contains no less than 5×10^4 atoms [26]. The most efficient way of producing large clusters involves the use of a supersonic slit nozzle [25] with a slit width of 500 μm; the transverse section of the cluster jet is rectangular-shaped. We note that additional ways of cluster plasma heating using auxiliary pulses during its expansion are presently under development [27]. The cluster size distribution and the fraction of atomic xenon in the cluster jet are special problems. There is no way of estimating the cluster size distribution by the Rayleigh scattering technique [24, 25]. In our calculation we rely on numerous experimental dependences of the electron plasma temperature on experimental conditions.

In the approach under discussion the beam of pump laser radiation should be directed perpendicular to the slit, so that the plasma length $L \approx 300$ μm. For a plasma volume of ~10^{-8} cm^3, the figure $N_{out}^{ph} \sim 10^{13}$ photons pulse^{-1} may be reached for $n_i = (2-3) \times 10^{19}$ cm^{-3} (see Fig. 3b for $L \sim$ 300 μm) and a pump pulse energy of ~10–20 mJ.

The reliability of the gains $g(t)$ obtained in our work for different plasma parameters and, as a consequence, the reliability of our estimate of the XRL photon yield are confirmed by comparison with the data of the corresponding experimental measurements of the time evolution $g(t)$ [13]. We note that these data were partly presented in our earlier paper [15].

A 41.8-nm Xe^{8+} XRL with the indicated cluster size and plasma density was described in the very first experiment to make an XRL in the plasma produced by laser irradiation of a cluster jet [12]. However, the single-pulse scheme of this work made use of neither an axicon nor an HOH, so that the plasma was rather nonuniform along the radius. The pump laser beam and the XRL radiation were strongly defocused in the propagation through the rather long plasma ($L =$ 1.7 mm). The XRL energy was expended for the heating of cluster layers adjacent to the plasma. This may be seen from the inset of Fig. 3 from Ref. [12]. The output XRL pulse for the highest atomic density (~3.3×10^{19} cm^{-3}) nevertheless turned out to be intense enough to be recorded.

We believe that an experimental facility made for the generation of an ultrashort pulse of Xe^{8+} XRL radiation should produce three Ti:sapphire laser pulses. The first pulse is intended for plasma pumping in the cluster jet, the second pulse should pass through a delay line and serve to generate the HOH, and the third one should pass through the second delay line to produce an ultrafast shutter which absorbs the residual radiation ~1 ps after the onset of X-ray lasing. For

the Xe^{8+} XRL with $\lambda = 41.8$ nm advantage is usually taken of an aluminium filter – a 300–400 nm thick foil. The second delay line provides a radiation pulse for the ultrafast ionisation (explosion) of the outer part of the foil filter, which transforms it to a low-temperature plasma capable of absorbing the residual part of the radiation from the active plasma region. Modern delay lines ensure an accuracy of the order of several femtoseconds. (For instance, the delay line in the experiment of Ref. [13] was made accurate to 7 fs for synchronising the HOH radiation pulse with the onset of X-ray lasing.) The ultrafast shutter provides a sharp termination of the XRL pulse.

The experiments of Refs [20–23] suggest that the plasma is produced in the cluster jet immediately after its irradiation by the pump pulse. For a high plasma density the intensity of X-ray lasing attains its maximum within several hundred femtoseconds (see Fig. 3a). Therefore, in the XRL scheme under consideration it is possible to produce an output pulse with an extremely steep leading edge and without a pedestal. This pulse shape holds promise for studying ultrafast processes. The scheme of the experimental facility will be detailed in one of our subsequent papers.

References

1. Barty A. et al. *Nat. Photonics*, **2**, 415 (2008).
2. Marchesini S. *Nat. Photonics*, **2**, 560 (2008).
3. Klisnick A. et al. *Phys. Rev. A*, **65**, 033810 (2002).
4. Zeitoun Ph. et al. *Nature (London)*, **431**, 426 (2004).
5. Wang Y., Granados E., Larotonda M.A., Berrill M., Luther B.M., Patel D., Menoni C.S., Rocca J.J. *Phys. Rev. Lett*., **97**, 123901 (2006).
6. Wang Y., Granados E., Pedaci F., Alessi D., Luther B., Berril M., Rocca J.J. *Nat. Photonics*, **2**, 94 (2008).
7. Hasegava N. et al. *Phys. Rev. A*, **76**, 043805 (2007).
8. Pedaci F. et al. *Opt. Lett*., **33**, 491 (2008).
9. Wang Y., Berrill M., Pedaci F., Shakya M.M., Gilbertson S., Zenghu Chang, Granados E., Luther B.M., Larotonda M.A., Rocca J.J. *Phys. Rev. A*, **79**, 023810 (2009).
10. Chou M.-C., Lin P.-H., Lin C.-A., Lin J.-Y., Wang J., Chen S.-Y. *Phys. Rev. Lett*., **99**, 063904 (2007).
11. Lin P.-H., Chou M.-C., Jiang M.-J., Tseng P.-C., Chu H.-H., Lin J.-Y., Wang J., Chen S.-Y. *Opt. Lett*., **34**, 3562 (2009).
12. Chu H.-H., Tsai H.-E., Chou M.-C., Yang L.-S., Lin J.-Y., Lee C.-H., Wang J., Chen S.-Y. *Phys. Rev. A*, **71**, 061804 (2005).
13. Mocek T., Sebban S., Maynard G., Zeitoun Ph., Faivre G., Hallou A., Fajardo M., Kazamias S., Cros B., Aubert D., de Lachèze-Murel G., Rousseau J.P., Dubau J. *Phys. Rev. Lett*., **95**, 173902 (2005).
14. Ivanova E.P. *Proc. 8th Int. Conf. on X-ray Lasers* (Melville, NY, AIP, 2002).
15. Ivanova E.P., Ivanov A.L. *Kvantovaya Elektron*., **34**, 1013 (2004) [*Quantum Electron*., **34**, 1013 (2004)].
16. Ivanova E.P. *Phys. Rev. A*, **84**, 043829 (2011).
17. Ivanova E.P., Zinoviev A.N. *Phys. Lett. A*, **274**, 239 (2000).
18. Lemoff B.E., Yin G.Y., Gordon C.L. III, Barty C.P.J., Harris S.E. *Phys. Rev. Lett*., **74**, 1574 (1995).
19. Sebban S. et al. *Phys. Rev. Lett*., **86**, 3004 (2001).
20. Ditmire T., Smith R.A., Tish W.G., Hutchinson M.H.R. *Phys. Rev. A*, **78**, 3121 (1997).
21. Shao Y.L., Ditmire T., Tisch J.W.G., Springate E., Marangos J.P., Hutchinson M.H.R. *Phys. Rev. Lett*., **77**, 3343 (1996).
22. Ditmire T., Donelly T., Rubenchik A.M., Falcone R.W., Perry M.D. *Phys. Rev. A*, **53**, 3379 (1996).
23. Ter-Avetisyan S., Vogt U., Stiel H., Schnürer M., Will I., Nickles P.V. *J. Appl. Phys*., **94**, 5489 (2003).
24. Hagena O.F., Obert W. *J. Chem. Phys*., **56**, 1793 (1972).
25. Chen G., Kim B., Ahn B., Kim D.E. *J. Appl. Phys*., **106**, 053507 (2009).
26. Springate E., Hay N., Tisch J.W.G., Mason M.B., Ditmire T., Hutchinson M.H.R., Marangos J.P. *Phys. Rev. A*, **61**, 063201 (2000).
27. Döppner T., Fennel Th., Diederich Th., Tiggesbäumker J., Meiwes-Broer K.H. *Phys. Rev. Lett*., **94**, 013401 (2005).